Received: 7 May 2023 | Revised: 1 September 2023 | Accepted: 8 September 2023

DOI: 10.1002/hbm.26493

RESEARCH ARTICLE

WILEY

A metabolism-functional connectome sparse coupling method to reveal imaging markers for Alzheimer's disease based on simultaneous PET/MRI scans

Luyao Wang[1] | Huanyu Xu[2] | Min Wang[1] | Matthias Brendel[3] | Axel Rominger[4] | Kuangyu Shi[4] | Ying Han[5,6,7,8] | Jiehui Jiang[1]

[1]School of Life Sciences, Shanghai University, Shanghai, China

[2]School of Communication and Information Engineering, Shanghai University, Shanghai, China

[3]Department of Nuclear Medicine, University Hospital of Munich, Ludwig Maximilian University of Munich, Munich, Germany

[4]Department of Nuclear Medicine, Inselspital, University Hospital Bern, Bern, Switzerland

[5]Department of Neurology, Xuanwu Hospital of Capital Medical University, Beijing, China

[6]Center of Alzheimer's Disease, Beijing Institute for Brain Disorders, Beijing, China

[7]National Clinical Research Center for Geriatric Disorders, Beijing, China

[8]Hainan University, Haikou, China

Correspondence
Jiehui Jiang, Institute of Biomedical Engineering, School of Life Science, Shanghai University, Shanghai, 200444, China.
Email: jiangjiehui@shu.edu.cn

Funding information
Shanghai Science and Technology Development Foundation, Grant/Award Number: 22YF1413900; National Natural Science Foundation of China, Grant/Award Numbers: 62303295, 62376150, 62206165; Science and Technology Innovation 2030—Major Projects, Grant/Award Number: 2022ZD021600

Abstract

Abnormal glucose metabolism and hemodynamic changes in the brain are closely related to cognitive function, providing complementary information from distinct biochemical and physiological processes. However, it remains unclear how to effectively integrate these two modalities across distinct brain regions. In this study, we developed a connectome-based sparse coupling method for hybrid PET/MRI imaging, which could effectively extract imaging markers of Alzheimer's disease (AD) in the early stage. The FDG-PET and resting-state fMRI data of 56 healthy controls (HC), 54 subjective cognitive decline (SCD), and 27 cognitive impairment (CI) participants due to AD were obtained from SILCODE project (NCT03370744). For each participant, the metabolic connectome (MC) was constructed by Kullback–Leibler divergence similarity estimation, and the functional connectome (FC) was constructed by Pearson correlation. Subsequently, we measured the coupling strength between MC and FC at various sparse levels, assessed its stability, and explored the abnormal coupling strength along the AD continuum. Results showed that the sparse MC–FC coupling index was stable in each brain network and consistent across subjects. It was more normally distributed than other traditional indexes and captured more SCD-related brain areas, especially in the limbic and default mode networks. Compared to other traditional indices, this index demonstrated best classification performance. The AUC values reached 0.748 (SCD/HC) and 0.992 (CI/HC). Notably, we found a significant correlation between abnormal coupling strength and neuropsychological scales ($p < .05$). This study provides a clinically relevant tool for hybrid PET/MRI imaging, allowing for exploring imaging markers in early stage of AD and better understanding the pathophysiology along the AD continuum.

KEYWORDS

coupling, functional connectome, metabolic connectome, simultaneous PET/fMRI, subjective cognitive decline

1 | INTRODUCTION

Alzheimer's disease (AD) is quickly becoming one of the most expensive, lethal, and burdening diseases with no curative treatments (Jessen et al., 2020). Early detection and intervention may slow down the continuous deterioration associated with AD. Subjective cognitive decline (SCD) has been regarded as the earliest symptomatic stage along the AD continuum (Jessen, Amariglio et al., 2020). Currently, the clinical diagnosis of SCD is largely based on self-reported symptoms from patients without objective evidence. Besides classical markers like amyloid-β (Aβ) and carrying of Apolipoprotein E (ApoE) ε4 gene (Yu et al., 2021), alterations in brain function due to AD may occur before memory impairment (Balsis et al., 2018). Investigating brain functional abnormalities in SCD individuals could provide a better understanding on primary cause of cognitive deficits and offer diagnostic imaging markers.

It has been shown that the [^{18}F] fluorodeoxyglucose positron emission tomography (^{18}F-FDG PET) imaging (Drzezga, Altomare et al., 2018; Scheef et al., 2012) and resting-state functional magnetic resonance imaging (rs-fMRI) (Hafkemeijer et al., 2012; Klaassens et al., 2017) are sensitive to neuronal functional activity degeneration in AD patients. However, the abnormal patterns reported in one modality (FDG-PET or rs-fMRI) were not entirely consistent across studies, especially in the early stage of SCD patients (Wang, Huang, et al., 2020). Signal of rs-fMRI arises from hemodynamic mechanisms in relation to oxygen consumption, while FDG-PET offers high sensitivity and a stable signal of glucose utilization (Sander et al., 2013). Researchers have found the utilization of oxygen and glucose by active neural cells in the brain are inextricably linked (Lourenco et al., 2015). Using the simultaneous ^{18}F-FDG PET and rs-fMRI scanner, researchers captured different aspects of functional brain activity for patients with AD at the group level (Ripp et al., 2020). Integrating complementary information from two modalities at the same brain state may help us further understand how impairments in neuronal function contribute to the mechanisms underlying AD in the SCD stage.

By measuring voxel-based correlations between glucose consumption and functional activity, researchers found reduced bioenergetic coupling in amnestic mild cognitive impairment (CI) patients (Marchitelli et al., 2018). Previous studies also reported better diagnostic performance for preclinical AD by using voxel-based coupling value of these two modalities (Ding et al., 2021). Although these studies revealed distribution differences of coupling values in specific brain areas, they ignored connections across separated brain areas. The AD is a disconnection syndrome that could be represented by brain networks (Gao et al., 2020; Wang, Huang, et al., 2020). Recent study reported strong glucose metabolism in brain areas with high functional connection in healthy male Lewis rats (Palombit et al., 2022). Although hybrid PET/MRI has been clinically used, how to integrate signal of these two modalities at brain network level is still unknown, preventing our understanding of stage-dependent effects on the functional brain activity along AD continuum.

Therefore, we introduce a metabolism-functional connectome (MC-FC) coupling method for hybrid PET/MRI imaging, which was conducted using a series of sparse thresholds to control false connections. The data of health control (HC), SCD, and cognitive impairments (CI) individuals were collected from hybrid PET/MRI scanners. It is of note that the MC and FC were constructed at individual level with the same network node. We not only validated the stability of the sparse MC–FC coupling index but also explored its abnormalities associated with AD. We hypothesize that the MC–FC coupling indices could capture AD-related pathological imaging biomarkers in SCD population. Results of our study are likely to provide insights into the development of clinically relevant tools for hybrid PET/MRI imaging, which could be used for the early diagnosis of AD.

2 | MATERIALS AND METHODS

2.1 | Sparse MC–FC coupling analytic method

The flowchart for the sparse MC–FC coupling analysis is presented in Figure 1. We used the Schaefer fMRI atlas to divide each brain into 400 regions of interest (ROIs) (Schaefer et al., 2018). Then, the MC adjacency matrix was constructed based on Kullback–Leibler divergence similarity estimation (KLSE; Wang, Jiang et al., 2020), while the FC adjacency matrix was estimated using Pearson correlation (Brier et al., 2014). The MC/FC adjacency matrix describes pairwise ROIs metabolic/functional connectivity. At different sparsity levels, we quantified MC–FC coupling index of each ROI by calculating the Spearman rank correlation between corresponding MC and FC values. The details are explained below.

MC estimation. For the MC, the probability density function (PDF) was estimated by nonparametric kernel density estimation for each voxel based on FDG-SUVR map. The characteristic function was calculated as follows:

$$\widehat{\varphi}(t) = \frac{1}{n}\sum_{j=1}^{n} e^{itx_j}, \tag{1}$$

where x_j represents an array quantifying the metabolic intensity of each voxel within the ROI. To avoid the issue of diverging integral, we used the Gaussian function as a damping function:

$$\psi(t) = e^{-\pi t^2}. \tag{2}$$

Next, the density estimation is derived using the Fourier transform formula and the following equation:

$$\widehat{f}(x) = \frac{1}{2\pi}\int_{-\infty}^{+\infty} \widehat{\varphi}(t)\psi_h(t)e^{-itx}dt = \frac{1}{nh}\sum_{j=1}^{n} K\left(\frac{x - x_j}{h}\right), \tag{3}$$

where K is the Fourier transform of the damping function. For each participant, the similarity of brain glucose metabolism was described by calculating the KLSE of PDFs between pairwise ROIs, which

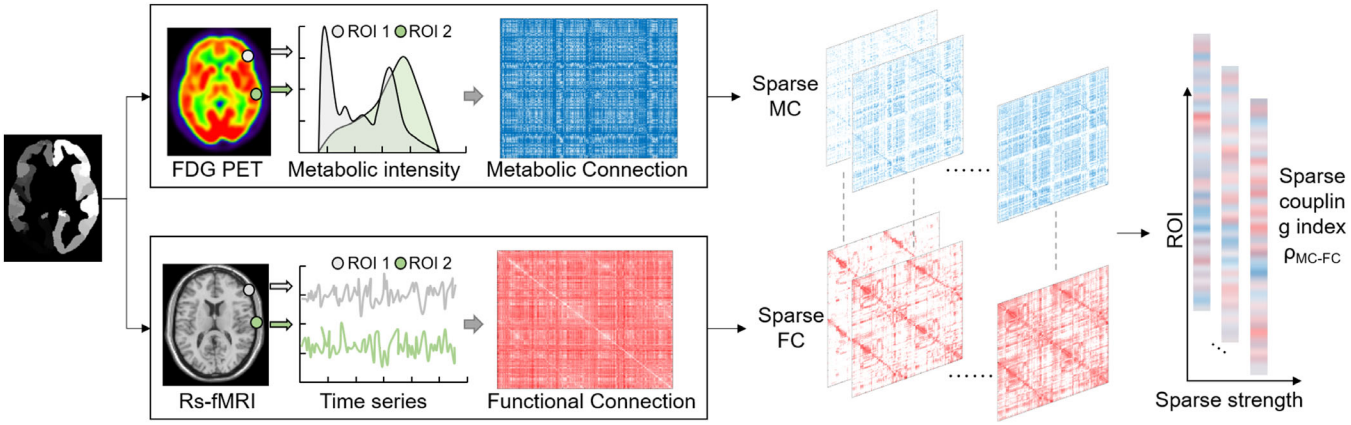

FIGURE 1 The flowchart of sparse MC–FC coupling analytic method. (a) The template was used to divide the brain into 400 regions of interest (ROIs). (b)The glucose metabolic connectome (MC) between two ROIs was estimated based on Kullback–Leibler divergence similarity estimation (KLSE) method, while functional connectome (FC) was estimated by Pearson correlation. (c) The MC–FC coupling index of each ROI was calculated according to Spearman-rank correlation between MC and FC at different threshold. Then, the coupling values with various sparsity were obtained.

wasinterpreted as metabolic connection. The KLSE is derived by transforming the symmetric KL divergence into an exponential form (relative entropy), which can be expressed mathematically as follows:

$$\mathrm{KLS}(P\,||Q) = e^{-\int_X \left(P(x)\log\frac{P(x)}{Q(x)}+Q(x)\log\frac{Q(x)}{P(x)}\right)dx)}, \quad (4)$$

where P and Q represent the PDFs of voxel intensities in a pair of ROIs. Finally, a 400 × 400 adjacency MC matrix was obtained.

FC estimation. For the FC, the mean fMRI time series of 400 ROIs were extracted regionally. The Pearson correlation coefficient was estimated between the time series of paired ROIs' to quantify the FC:

$$\mathrm{FC}_{(X,Y)} = \frac{\sum_{i=1}^{n}(X_i-\overline{X})(Y_i-\overline{Y})}{\sqrt{\sum_{i=1}^{n}(X_i-\overline{X})^2\sum_{i=1}^{n}(Y_i-\overline{Y})^2}}, \quad (5)$$

where X and Y are the mean time series of ROIs per pair, and $\overline{X}$ and $\overline{Y}$ are the mean values of X and Y, respectively. For each subject, a 400 × 400 weighted adjacency FC matrix was constructed.

Sparse MC–FC coupling index. To remove spurious connection and to obtain sparsely connected matrices, we used proportional threshold to ensure equal density across patient and control samples. The sparsity was defined as the ratio of the actual edge number to the total connected edge number in the MC and FC network. The range of sparsity (0.1–0.5, interval = 0.01) was defined to guarantee that the resulting random graph was connected, with a significance level of $p < .05$ for correlation coefficients (Li, Biswal, et al., 2019). However, different thresholds produce different numbers of remaining connections, which may influence the coupling values. It is not all clear what density is the most accurate for inferring brain connection (van den Heuvel et al., 2017). To avoid the issues, we calculated the averaged coupling index $a\rho_{\mathrm{MC-FC}}$ to avoid the influence of specific threshold for further analysis. The sparse MC–FC coupling index was calculated as follows:

$$a\rho_{\mathrm{MC-FC}} = \frac{\sum_{n=1}^{s} r_n(\mathrm{MC},\mathrm{FC})}{s}, \quad (6)$$

where s represents the amount of sparsity. The r represents the coupling value calculated by Spearman-rank correlation between MC and FC at specific threshold. Then, the $a\rho_{\mathrm{MC-FC}}$ coupling values were normalized by calculating the Z-scores across ROIs. Therefore, each participant had a one-dimensional vector that represented the regional sparse coupling strength of 400 ROIs.

2.2 | Participants

Participants in this retrospective study were recruited from the Chinese Sino Longitudinal Study on Cognitive Decline project (ClinicalTrials.gov: NCT03370744) from 2018 to now (Li, Wang, et al., 2019). In this retrospective study, participants with image quality problems and excessive head movement (>3 mm or >3°) were excluded. This resulted in a total of, 137 participants, including 56 healthy control (HC), 54 SCD, and 27 CI individuals (see Supplemental Figure S1). All the participants signed written informed consent and underwent the neuropsychological scales, including the mini mental state examination (MMSE) and Montreal cognitive assessment-basic (MoCA-B) to assess cognitive function, Hamilton depression scale (HAMD) and Hamilton anxiety scale (HAMA) to assess depression and anxiety levels. Details of the inclusion and exclusion criteria can be found in the Supplemental Method. The project was approved by the Ethics Committee of Xuanwu Hospital of Capital Medical University according to the Helsinki Declaration.

2.3 | Image protocol and data preprocessing

The simultaneous ^{18}F-FDG-PET (scan duration = 35 min, 8 iterations), rs-fMRI (echo time [TE] = 30 ms, repetition time [TR] = 2000 ms), structural T1-weighted MRI (TE = 2.98 ms, TR = 6.9 ms) data were obtained from a hybrid 3.0 T TOF PET/MR scanner (SIGNA PET/MR, GE Healthcare, Milwaukee, Wisconsin, USA). The PET and rs-fMRI data were preprocessed by the SPM12 (https://www.fil.ion.ucl.ac.uk/spm) and DPARSF (http://www.rfmri.org/dpabi) toolbox respectively in MATLAB 2016b (MathWorks, Natick, Mass). More details on the scan parameters and data preprocessing were provided in Supplemental Method.

2.4 | Validation of sparse MC–FC coupling index

We validated the robustness of MC–FC coupling index across subjects in HC group. First, we determined 1000 null models of MC and FC, respectively, at different sparsity levels by shuffling the connection matrix while preserving the overall degree- and weight-distribution (*null_model_und_sign.m* function in the brain connectivity toolbox). The null-distribution of coupling index was derived based on these shuffled MC and FC matrices, which could be used to infer statistical significance of true $a\rho_{MC-FC}$. In addition, we further validated the method by disrupting the order of brain regions in the MC and FC matrices for each subject separately.

Second, we divided 400 ROIs into seven networks: visual, somatomotor (SM), dorsal attention network (DAN), ventral attention network (VAN), limbic, frontoparietal control (FPCN), and default mode network (DMN; Schaefer et al., 2018). We calculated the histogram distribution of $a\rho_{MC-FC}$ in each network and measured the standard deviation across subjects as the individual variation. The distribution and variation of the coupling index were compared with the index derived from only one modality, either MC or FC. We also compared the $a\rho_{MC-FC}$ with voxel-based coupling method using Bland–Altman consistency analyses and histogram distribution. The voxel-based coupling method has been already explored in previous work and shown to be stable in the cognitive normal population (Ding et al., 2021), including (a) correlation between SUVR and the fractional amplitude of low-frequency fluctuations (fALFF), and (b) correlation between SUVR and the regional homogeneity (ReHo).

2.5 | Abnormal sparse coupling index along the AD continuum

To investigate whether AD has stage-dependent effects on the coupling of metabolic and functional connections, the one-way analysis of variance (ANOVA) analysis was performed across HC, SCD, and CI groups in each brain network. The least significant difference (LSD) test was utilized for post hoc pairwise analysis. The network showed significant differences that could be considered as imaging markers for early diagnosis of AD. We also compared the one modality MC and FC across HC, SCD, and CI groups in each brain network in the same way.

Furthermore, we developed a logistic regression (LR) model to evaluate the classification performance of 7 networks' $a\rho_{MC-FC}$ for distinguishing SCD and CI from HC. The results were compared with one-modality indexes (MC, FC, SUVR, fALFF, ReHo) and voxel-based coupling indexes of two modalities (SUVR-fALFF and SUVR-ReHo). Furthermore, we evaluated the potential AD-related pathological significance of these brain networks. The partial correlation coefficients between $a\rho_{MC-FC}$ and clinical scale scores of SCD and CI patients were calculated controlling for gender, age, and education.

2.6 | Statistical analysis

Clinical and demographic characteristics were compared between groups using the chi-square test for categorical data and the one-way ANOVA for continuous data. We used one-way ANOVA to compare $a\rho_{MC-FC}$ across three HC, SCD, and CI groups with LSD post hoc analysis. All the statistical analyses were performed in SPSS (version 25.0, IBM). The *p*-values were set to .05 (two-tailed) after false discovery rate (FDR) correction. The LR analysis was performed in GraphPad Prism (version 9.3.1, GraphPad Software). The receiver operating characteristic curve (ROC) analysis and its area under the curve (AUC) with 95% confidence interval (CI) was calculated.

3 | RESULTS

3.1 | Demography and neuropsychology

The detailed demographic and clinical information of all groups are presented in Table 1. The Chi-square test of categorical variables showed that the gender of SCD was significantly different from HC

TABLE 1 Clinical and baseline demographic characteristics of all participants.

	HC	SCD	CI
Gender (M/F)	56 (24/32)	54 (9/45)[a]	27 (10/17)[b]
Age (years)	65.48 ± 4.21	66.02 ± 4.52	64.22 ± 10.18
Education	12.87 ± 2.81	13.15 ± 2.66	12.89 ± 3.80
MMSE	29.32 ± 0.83	29.09 ± 0.80	19.48 ± 5.80[b,c]
MOCA-B	26.41 ± 1.97	26.43 ± 1.68	13.11 ± 6.18[b,c]
HAMD	1.88 ± 2.20	3.65 ± 3.48[a]	6.74 ± 5.57[b,c]
HAMA	3.00 ± 2.62	4.83 ± 3.47[a]	6.33 ± 6.28[c]

Note: Data are given as mean ± standard deviation.
Abbreviations: CI, cognitive impairment; HAMD, Hamilton depression rating scale; HAMA, Hamilton anxiety rating scale; HC, healthy control; MMSE, mini-mental state examination; MoCA-B, basic version of Montreal cognitive assessment; SCD, subjective cognitive decline.
[a]$p < .05$ HC versus SCD.
[b]$p < .05$ SCD versus CI.
[c]$p < .05$ HC versus CI.

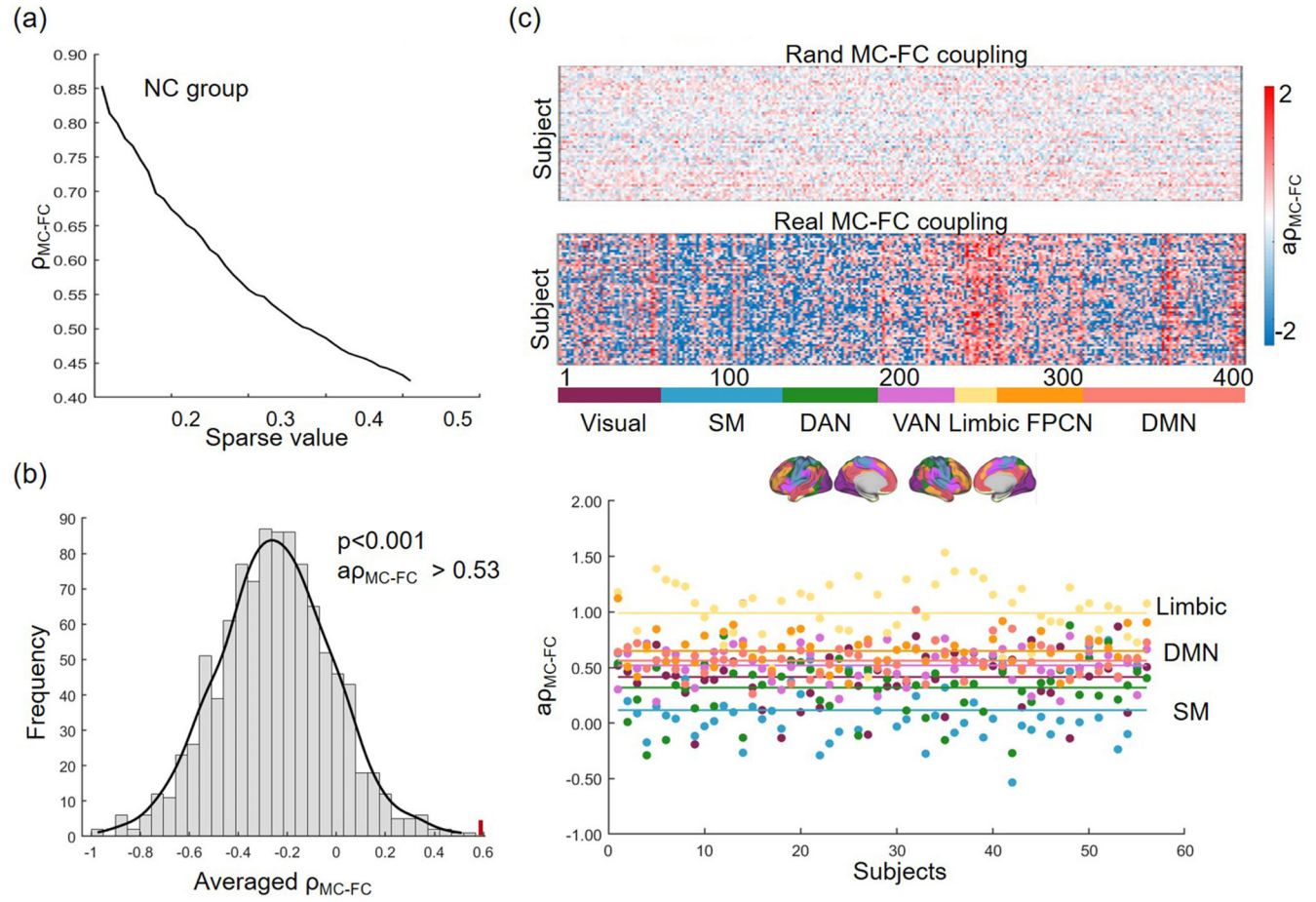

FIGURE 2 Reliability analysis of MC–FC coupling method in the HC group. (a) The coupling value at different sparsity. (b) The null-distribution of coupling value $a\rho_{MC-FC}$ from rewired null-model network. (c) Averaged coupling value across different sparsity in each brain areas in each subject.

and CI groups. For continuous variables, no significant difference was found in age or education among the three groups. The MMSE and MOCA-B scores in the CI group were significantly lower than those in HC and SCD groups ($p < .001$, two-sample t-test, FDR corrected). The HAMD scale score showed significant differences among the three groups. Compared with the HC group, the HAMA scores of the SCD and CI groups were significantly higher.

3.2 | Validation of sparse MC–FC coupling method

The coupling index decreased as the sparsity increased (Figure 2a). To avoid the influence of a specific threshold, we computed the averaged value and compared it with the null distribution of $a\rho_{MC-FC}$. This could account for the likelihood of observing $a\rho_{MC-FC}$ by chance, resulting in a significant p-value of $p < .001$ (Figure 2b). In addition, we observed that coupling index in brain areas was consistent across subjects. The consistent was disrupted when analyzing rand MC–FC coupling based on disrupted brain areas. Specifically, the limbic network showed the highest coupling ($a\rho_{MC-FC} = 0.990$, one-sample t-test $p < .001$), followed by the DMN, while the SM network showed the lowest coupling strength ($a\rho_{MC-FC} = 0.116$, one-sample t-test $p = .003$; Figure 2c).

Compared to one modality MC and FC, the $a\rho_{MC-FC}$ was more normally distributed in each network, especially in DAN [main effect of one-way ANOVA analysis, $p = .001$, $F(2,165) = 7.925$], VAN [$p < .001$, $F(2,165) = 29.931$], limbic [$p = 0.03$, $F(2,165) = 3.596$], FPCN [$p < .001$, $F(2,165) = 35.358$] and DMN [$p = .007$, $F(2,165) = 5.102$] network (Figure 3). The index with normally distribution could minimize the influence of noise. Then, the index could be used to explore the imaging markers with disease specificity. The individual variability of $a\rho_{MC-FC}$ (visual: 0.250, SM:0.272, DAN: 0.246, VAN: 0.166, limbic: 0.262, FPCN: 0.156, DMN: 0.139) was higher than MC but lower than FC.

Based on Bland–Altman analyses, the $a\rho_{MC-FC}$ was consistent with voxel-based coupling indexes of SUVR-fALFF and SUVR-ReHo, with mean differences of 0.048 and 0.064, respectively. The $a\rho_{MC-FC}$ also showed a more normal distribution in visual [$p = .001$, $F(2,165) = 7.632$], SM[$p < .001$, $F(2,165) = 14.755$], DAN[$p < .001$, $F(2,165) = 82.647$], VAN[$p < .001$, $F(2,165) = 135.554$], limbic[$p < .001$, F

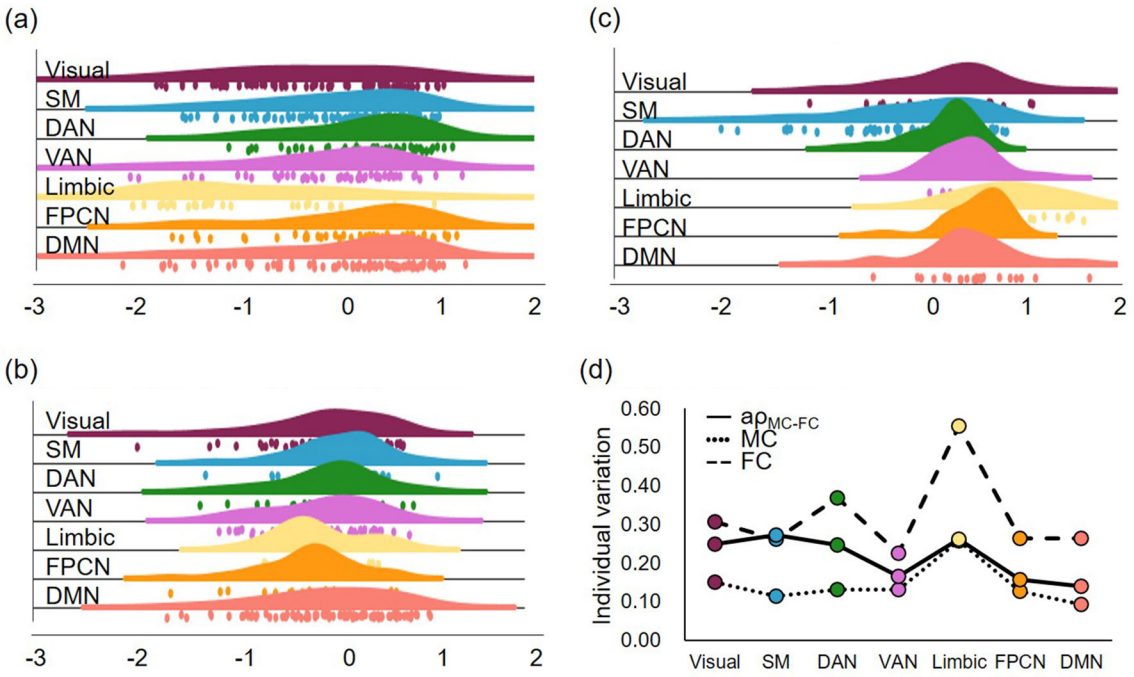

FIGURE 3 Comparison of one modality MC, FC and coupling value. The histogram distribution of (a) MC, (b) FC, (c) $a\rho_{MC-FC}$ in each brain network. (d) The individual variation of MC, FC, and $a\rho_{MC-FC}$ in each brain network.

(2,165) = 46.277], FPCN[$p < 0.001$, $F(2,165) = 208.526$] and DMN [$p < .001$, $F(2,165) = 58.965$] network (Supplemental Figure S2).

3.3 | Imaging marker based on sparse MC–FC coupling index

The MC–FC coupling showed a decrease as the sparsity increased in three groups at each threshold (Supplemental Figure S3). The difference across three groups were similar at each sparsity. To avoid the influence of specific sparse threshold, the following comparisons were based on the averaged coupling index ($a\rho_{MC-FC}$). The one-way ANOVA suggested significant main-effect in SM [$p = .004$, $F(2,134) = 5.707$], limbic [$p < .001$, $F(2,134) = 8.851$], and DMN [$p < .001$, $F(2,134) = 18.437$] network (Figure 4a, b). Based on LSD post hos analysis, the CI group had the highest $a\rho_{MC-FC}$ in SM network, which was significant when compared to SCD ($p = .002$) and HC group ($p = .004$). In limbic network, compared with normal controls, the $a\rho_{MC-FC}$ was significantly increased in SCD ($p = .029$) and decreased in CI group ($p = .017$). There was a declining tendency across three groups in FPCN, and especially in DMN network (HC/SCD: $p = .041$, HC/CI: $p < .001$, SCD/CI: $p < .001$).

Results based on one modality, MC and FC, also showed some statistically significant differences across three groups (Figure 4b, c). The CI group had lower MC in DAN (CI vs. HC: $p = .01$; CI vs. SCD: $p = .003$), and FPCN (CI vs. HC: $p < .001$; CI vs. SCD: $p = .007$) when compared to HC and SCD, while having higher MC in limbic ($p < .001$). In addition, the CI group had lower FC in visual network compared to SCD ($p = .002$), and higher FC in FPCN compared to HC ($p = .041$) and SCD ($p = .003$).

3.4 | ROC analysis

We further assessed the diagnosis performance of $a\rho_{MC-FC}$ from 7 networks based on LR model analysis. The ROC analysis results for discriminating SCD and HC were displayed in Figure 5a. In comparison to the MC, FC, ReHo, fALFF, SUVR, SUVR-ReHo, and SUVR-fALFF, the $a\rho_{MC-FC}$ had the highest AUC value (AUC = 0.748, 95% CI = [0.645, 0.850]). When differentiating CI and HC, the MC–FC coupling also had the highest AUC value (AUC = 0.992, 95%CI = [0.978, 1.000]) compared to other indices (Figure 5b and Supplemental Table S1).

3.5 | Correlation analysis

Figure 6 showed results of correlation between MC–FC coupling strength $a\rho_{MC-FC}$ in the SM, limbic, DMN network and clinical scales controlling for age, gender, and education. The $a\rho_{MC-FC}$ was positively correlated with MMSE (SM: $r = -0.431$, $p < .001$; limbic: $r = -0.472$, $p < .001$; DMN: $r = .303$, $p = .026$, FDR corrected) and MoCA-B (SM: $r = -0.382$, $p = .004$; limbic: $r = 0.440$, $p < .001$; DMN: $r = 0.318$, $p = .025$, FDR corrected), while no other neuropsychological scale scores were significantly correlated (Figure 6 and Supplemental Table S2).

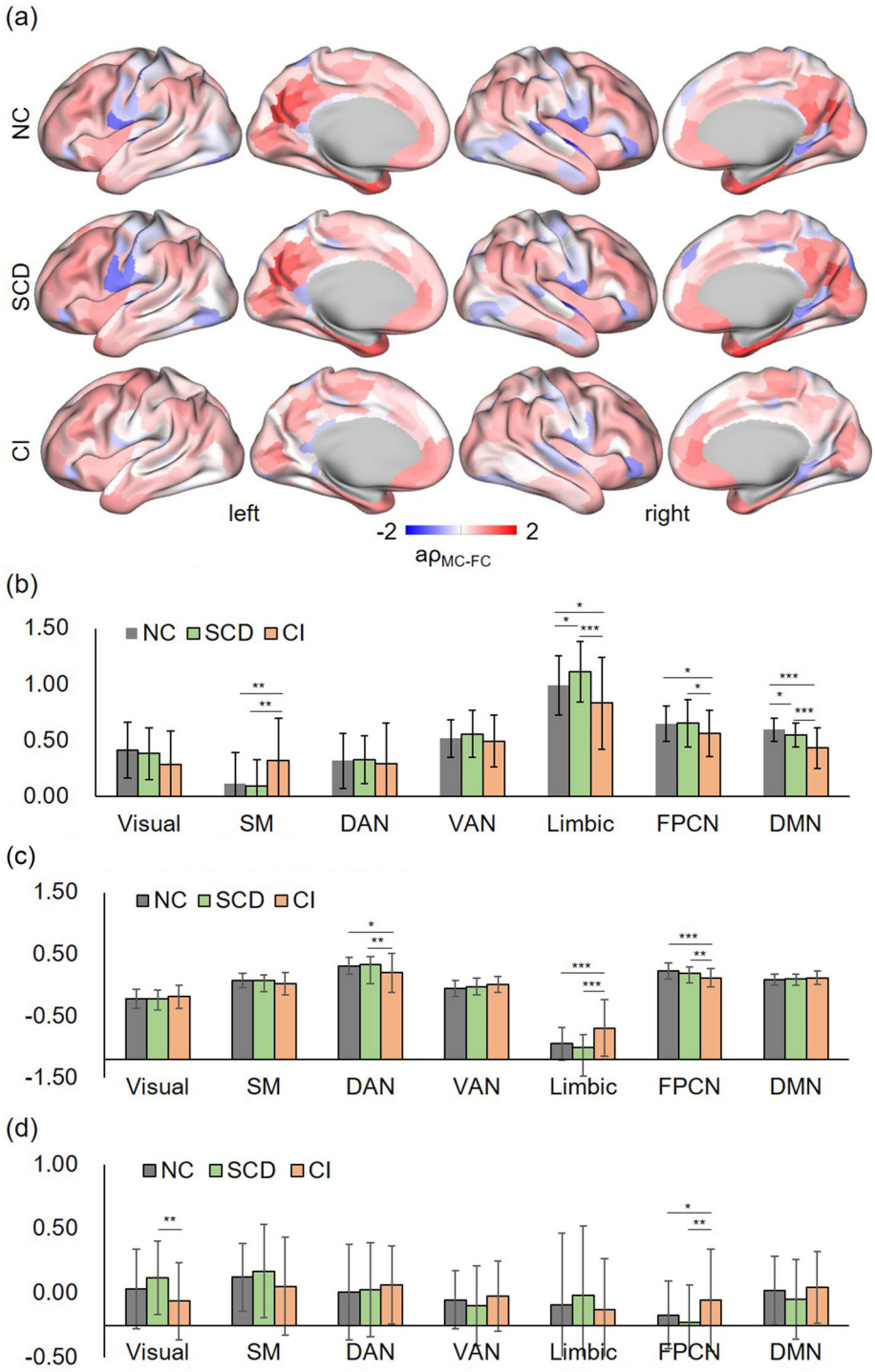

FIGURE 4 Results of abnormal areas along the AD continuum. (a) The mean coupling value of each brain areas in HC, SCD, and CI group. (b) Pairwise post hoc analysis results across three groups based on coupling value, (c) MC, and (d) FC index. $^{*}p < .05$, $^{**}p < .01$, $^{***}p < .001$.

4 | DISCUSSION

In this study, we propose a connectome-based method for hybrid PET/MRI imaging, which investigates the coupling relationship between sparse metabolic and functional networks at the individual level. Results showed the coupling index $a\rho_{MC-FC}$ was significantly higher than null-distribution with high consistency across subjects. It was more normally distributed than the result derived from one modality (MC or FC) or voxel-based coupling index. In addition, the $a\rho_{MC-FC}$ could detect more brain areas with significant differences across HC, SCD, and CI groups, especially in limbic and DMN network which was related to memory abilities. Based on the LR model, the $a\rho_{MC-FC}$ showed highest AUC value for distinguishing SCD and CI from HC. The networks (SM, limbic, DMN) with significant differences across the AD continuum were also significantly correlated to neuropsychological scales, which could be used as imaging markers for early detection of AD.

Simultaneous acquisition of fMRI and PET data could minimize the variability caused by changes in brain states or moods. We rewired the MC and FC matrices 1000 times to obtain the null-

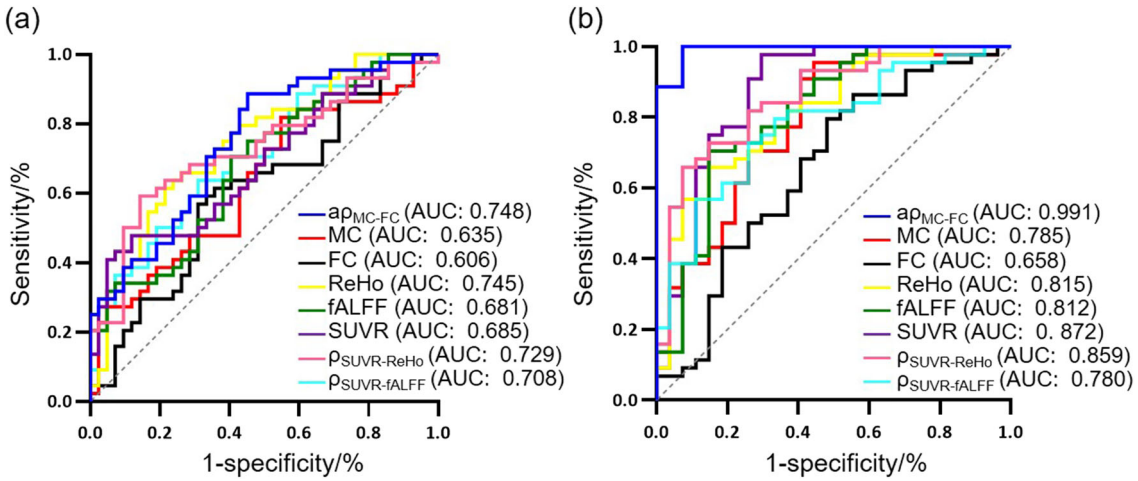

FIGURE 5 Receiver operating characteristic curve (ROC) curves. (a) Classification ROC curve of SCD and HC. (b) Classification ROC curve of CI and HC.

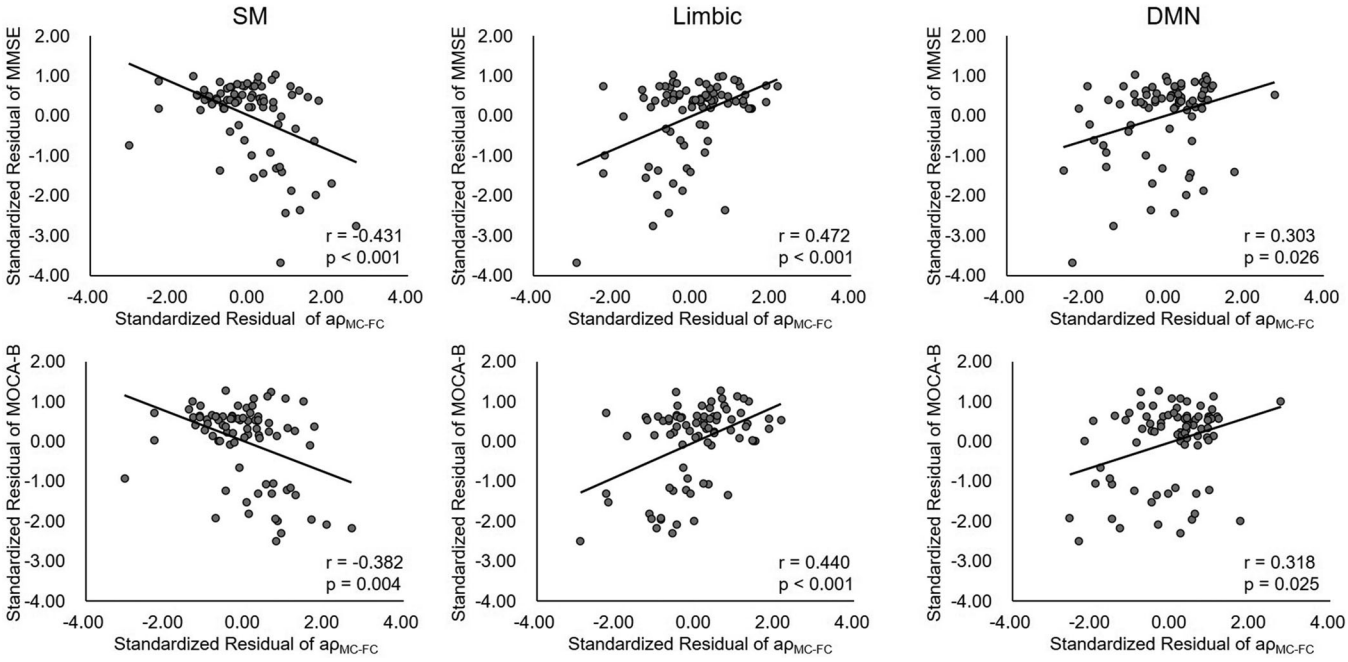

FIGURE 6 Results of partial correlation analysis between coupling value (in SM, limbic, and DMN network) and neuropsychological scales (MMSE and MOCA-B).

distribution of coupling index. Result supported the notion that the FDG PET and rs-fMRI represent similar aspects of functional brain activity which cannot be clearly separated. The coupling was high in limbic followed by DMN network. However, the SM network showed low coupling. An animal study reported a high coupling of functional and metabolic network organizations in DMN regions (Ripp et al., 2020). This may be attributed to the continuous coherent activity during resting state in these brain areas (Raichle et al., 2001). Based on histogram distribution and Bland–Altman plot analysis, result showed that the MC–FC coupling strength was stable and normally distributed in each brain network. The FC showed highest individual variation followed by $a\rho_{MC-FC}$ and the MC. This may be due to dynamic temporal fluctuations of FC. Results also indicated similar variation between $a\rho_{MC-FC}$ and MC in VAN, limbic, FPCN and DMN, despite the high variation of FC, demonstrating the stability of $a\rho_{MC-FC}$.

For CI patients, the $a\rho_{MC-FC}$ and one modality indexes (MC and FC) both identified abnormal changes in FPCN network. This finding is consistent with previous study that reported impaired FPCN of AD patients during verbal memory recall tasks (Dhanjal & Wise, 2014). In addition, researchers suggested that altered FC in FPCN may serve as a potential biomarker for the diagnose of AD (Zhao, Sang et al., 2019).

However, the proposed MC–FC coupling method enabled us to identify more SCD-related regions, including the limbic and DMN areas. Compared to one modality MC and FC, the use of $a\rho_{MC-FC}$ allowed for the characterization of the communication ability of brain from different perspectives. The MC can reflect brain energy consumption at slower temporal scales in the range of minutes, while FC can be derived from dynamic fluctuations on a temporal scale of seconds. Combining the MC and FC may synthesize different aspects of early-stage disease outcomes (Ripp et al., 2020).

Along the AD continuum, our results suggested that there was a reduction in the MC–FC coupling strength in the DMN for SCD and CI groups. The DMN has drawn a lot of interest in research about AD (Dillen et al., 2016; Dong et al., 2018; Viviano et al., 2019). Aggregation of Aβ protein preferentially affects DMN regions, which was associated with AD clinical performance (Palmqvist et al., 2017). Decreased coupling in the DMN network at the SCD stage maybe related to the early deposition of Aβ protein. Our finding was in agreement with the previous studies which had reported reduction coupling in DMN areas in amnestic MCI and AD (Shulman et al., 2001). However, their studies focused on voxel-based coupling methods and did not include SCD patients (Raichle et al., 2001). The DMN remained alert in resting state and maintained high demand for cerebral blood flow as well as metabolic activity in this study, which may be the main decoupling network in SCD individuals.

Reduced MC–FC coupling may result from neuronal integration and signaling failure due to AD Badhwar et al., 2017). During rest, the brain network derives most of its energy via oxidative phosphorylation (Shulman et al., 2001), leading to high coupling strength of MC–FC with a similar ratio of glucose consumption and oxygen utilization. Disruption in the synergistic utilization of oxygen and glucose utilization in the brain may be related to excessive aerobic glycolysis, which refers to the non-oxidative metabolism of glucose despite adequate oxygen being present (Bullmore & Sporns, 2012). Interestingly, our results demonstrated a significant increase in coupling within limbic network for SCD, which decreased in CI stage. Previous studies reported that the DMN and limbic network are two separate subunits of a memory circuit interacting to support memory-guided behavior (Ritchey et al., 2015). This result could be explained by the compensatory cognitive effect observed in the SCD stage (Wang, Jiang et al., 2020). A previous study reported increased glucose metabolism in the right medial temporal lobe in the SCD group, which was related to compensatory neuronal activity (Scheef et al., 2012).

Results of ROC analysis further suggested that the $a\rho_{MC-FC}$ had better classification performance than one modality and voxel-based coupling indexes. Based on voxel-based coupling with a comparable sample size, a prior study obtained an AUC of 0.660 (Ding et al., 2021). By using LASSO classifier, researches obtained an AUC of 0.75 based on magnetoencephalography scans, which was a similar value to this study (Lopez-Sanz et al., 2019). We further investigated the pathological value of MC–FC coupling and found significantly positive correlations between MC–FC coupling and neuropsychological scales (MMSE, MoCA-B). It meant that disrupted coupling relationships in these brain networks may play an important role in cognitive decline due to AD.

However, there are some limitations to this study. First, all connections and regions were treated equally in the process of sparse MC–FC coupling calculation. It is possible that functional and metabolic connection types differ among cortical regions, and therefore treating all connections and regions equally may not accurately capture the underlying biology. Future work may consider modifying MC–FC coupling measures, for example, to distinguish inhibitory connections from excitatory connections. Second, observed effects were interpreted on brain network levels. It is better to further explore the physiological mechanism in combination with animal experiments. Additionally, the small sample of participants in this study may be a limitation. Future studies could consider enrolling larger samples of patients or longitudinal SCD follow-up data to validate our results.

5 | CONCLUSION

The prolonged symptom-free stage of AD provides us with an opportunity to examine the brain changes that antedate cognitive decline. However, previous studies of neuroimaging markers only focused on one modality (FDG-PET or rs-fMRI) and being limited to group-level or voxel-based investigations. Based on hybrid PET/MRI imaging, we proposed a connectome-based sparse coupling method between glucose metabolic and functional connection at individual level. Stability and dissimilarity analysis of the MC–FC coupling strength in brain networks indicated that alterations in these patterns may be potential imaging markers for the early detection of AD at the SCD stage, especially in limbic and DMN areas. These results allow for new insights into the pathophysiology of SCD patients.

AUTHOR CONTRIBUTIONS

Luyao Wang, Huanyu Xu: Designed research, performed research, analyzed data, wrote the paper. **Min Wang:** Designed research, analyzed data. **Matthias Brendel, Axel Rominger:** Designed research. **Kuangyu Shi, Ying Han:** Wrote the paper. **Jiehui Jiang:** Performed research, wrote the paper.

ACKNOWLEDGMENTS

This work was supported by the Shanghai Science and Technology Development Foundation (Sailing Program) (22YF1413900), the National Natural Science Foundation of China (No. 62206165, 62376150, and 62303295), and Science and Technology Innovation 2030—Major Projects (No. 2022ZD021600).

CONFLICT OF INTEREST STATEMENT

The authors declare no competing interest.

DATA AVAILABILITY STATEMENT

The data that support the findings of this study are available on request from the corresponding author. The data are not publicly available due to privacy or ethical restrictions.

ORCID

Ying Han https://orcid.org/0000-0003-0377-7424

Jiehui Jiang https://orcid.org/0000-0003-4948-3683

REFERENCES

Badhwar, A., Tam, A., Dansereau, C., Orban, P., Hoffstaedter, F., & Bellec, P. (2017). Resting-state network dysfunction in Alzheimer's disease: A systematic review and meta-analysis. *Alzheimer's & Dementia*, *8*, 73–85.

Balsis, S., Geraci, L., Benge, J., Lowe, D. A., Choudhury, T. K., Tirso, R., Doody, R. S., & I. Alzheimer's Disease Neuroimaging. (2018). Statistical model of dynamic markers of the Alzheimer's pathological Cascade. *The Journals of Gerontology. Series B, Psychological Sciences and Social Sciences*, *73*(6), 964–973.

Brier, M. R., Thomas, J. B., Fagan, A. M., Hassenstab, J., Holtzman, D. M., Benzinger, T. L., Morris, J. C., & Ances, B. M. (2014). Functional connectivity and graph theory in preclinical Alzheimer's disease. *Neurobiology of Aging*, *35*(4), 757–768.

Bullmore, E., & Sporns, O. (2012). The economy of brain network organization. *Nature Reviews. Neuroscience*, *13*(5), 336–349.

Dhanjal, N. S., & Wise, R. J. (2014). Frontoparietal cognitive control of verbal memory recall in Alzheimer's disease. *Annals of Neurology*, *76*(2), 241–251.

Dillen, K. N. H., Jacobs, H. I. L., Kukolja, J., von Reutern, B., Richter, N., Onur, O. A., Dronse, J., Langen, K. J., & Fink, G. R. (2016). Aberrant functional connectivity differentiates retrosplenial cortex from posterior cingulate cortex in prodromal Alzheimer's disease. *Neurobiology of Aging*, *44*, 114–126.

Ding, C., Du, W., Zhang, Q., Wang, L., Han, Y., & Jiang, J. (2021). Coupling relationship between glucose and oxygen metabolisms to differentiate preclinical Alzheimer's disease and normal individuals. *Human Brain Mapping*, *42*(15), 5051–5062.

Dong, C., Liu, T., Wen, W., Kochan, N. A., Jiang, J., Li, Q., Liu, H., Niu, H., Zhang, W., Wang, Y., Brodaty, H., & Sachdev, P. S. (2018). Altered functional connectivity strength in informant-reported subjective cognitive decline: A resting-state functional magnetic resonance imaging study. *Alzheimer's & Dementia*, *10*, 688–697.

Drzezga, A., Altomare, D., Festari, C., Arbizu, J., Orini, S., Herholz, K., Nestor, P., Agosta, F., Bouwman, F., Nobili, F., Walker, Z., Frisoni, G. B., Boccardi, M., & EANM-EAN Task Force for the Prescription of FDG-PET for Dementing Neurodegenerative Disorders. (2018). Diagnostic utility of 18F-fluorodeoxyglucose positron emission tomography (FDG-PET) in asymptomatic subjects at increased risk for Alzheimer's disease. *European Journal of Nuclear Medicine and Molecular Imaging*, *45*(9), 1487–1496.

Gao, Z., Feng, Y., Ma, C., Ma, K., Cai, Q., & I. Alzheimer's Disease Neuroimaging. (2020). Disrupted time-dependent and functional connectivity brain network in Alzheimer's disease: A resting-state fMRI study based on visibility graph. *Current Alzheimer Research*, *17*(1), 69–79.

Hafkemeijer, A., van der Grond, J., & Rombouts, S. A. (2012). Imaging the default mode network in aging and dementia. *Biochimica et Biophysica Acta*, *1822*(3), 431–441.

Jessen, F., Amariglio, R. E., Buckley, R. F., van der Flier, W. M., Han, Y., Molinuevo, J. L., Rabin, L., Rentz, D. M., Rodriguez-Gomez, O., Saykin, A. J., Sikkes, S. A. M., Smart, C. M., Wolfsgruber, S., & Wagner, M. (2020). The characterisation of subjective cognitive decline. *Lancet Neurology*, *19*(3), 271–278.

Jia, L., Quan, M., Fu, Y., Zhao, T., Li, Y., Wei, C., Tang, Y., Qin, Q., Wang, F., Qiao, Y., Shi, S., Wang, Y. J., Du, Y., Zhang, J., Zhang, J., Luo, B., Qu, Q., Zhou, C., Gauthier, S., … C. Group for the Project of Dementia Situation. (2020). Dementia in China: Epidemiology, clinical management, and research advances. *Lancet Neurology*, *19*(1), 81–92.

Klaassens, B. L., van Gerven, J. M. A., van der Grond, J., de Vos, F., Moller, C., & Rombouts, S. (2017). Diminished posterior precuneus connectivity with the default mode network differentiates Normal aging from Alzheimer's disease. *Frontiers in Aging Neuroscience*, *9*, 97.

Li, J., Biswal, B. B., Wang, P., Duan, X., Cui, Q., Chen, H., & Liao, W. (2019). Exploring the functional connectome in white matter. *Human Brain Mapping*, *40*(15), 4331–4344.

Li, X., Wang, X., Su, L., Hu, X., & Han, Y. (2019). Sino longitudinal study on cognitive decline (SILCODE): Protocol for a Chinese longitudinal observational study to develop risk prediction models of conversion to mild cognitive impairment in individuals with subjective cognitive decline. *BMJ Open*, *9*(7), e028188.

Lopez-Sanz, D., Bruna, R., Delgado-Losada, M. L., Lopez-Higes, R., Marcos-Dolado, A., Maestu, F., & Walter, S. (2019). Electrophysiological brain signatures for the classification of subjective cognitive decline: Towards an individual detection in the preclinical stages of dementia. *Alzheimer's Research & Therapy*, *11*(1), 49.

Lourenco, C. F., Ledo, A., Dias, C., Barbosa, R. M., & Laranjinha, J. (2015). Neurovascular and neurometabolic derailment in aging and Alzheimer's disease. *Frontiers in Aging Neuroscience*, *7*, 103.

Marchitelli, R., Aiello, M., Cachia, A., Quarantelli, M., Cavaliere, C., Postiglione, A., Tedeschi, G., Montella, P., Milan, G., Salvatore, M., Salvatore, E., Baron, J. C., & Pappata, S. (2018). Simultaneous resting-state FDG-PET/fMRI in Alzheimer disease: Relationship between glucose metabolism and intrinsic activity. *NeuroImage*, *176*, 246–258.

Palmqvist, S., Scholl, M., Strandberg, O., Mattsson, N., Stomrud, E., Zetterberg, H., Blennow, K., Landau, S., Jagust, W., & Hansson, O. (2017). Earliest accumulation of beta-amyloid occurs within the default-mode network and concurrently affects brain connectivity. *Nature Communications*, *8*(1), 1214.

Palombit, A., Silvestri, E., Volpi, T., Aiello, M., Cecchin, D., Bertoldo, A., & Corbetta, M. (2022). Variability of regional glucose metabolism and the topology of functional networks in the human brain. *NeuroImage*, *257*, 119280.

Raichle, M. E., MacLeod, A. M., Snyder, A. Z., Powers, W. J., Gusnard, D. A., & Shulman, G. L. (2001). A default mode of brain function. *Proceedings of the National Academy of Sciences of the United States of America*, *98*(2), 676–682.

Ripp, I., Stadhouders, T., Savio, A., Goldhardt, O., Cabello, J., Calhoun, V., Riedl, V., Hedderich, D., Diehl-Schmid, J., Grimmer, T., & Yakushev, I. (2020). Integrity of neurocognitive networks in dementing disorders as measured with simultaneous PET/functional MRI. *Journal of Nuclear Medicine*, *61*(9), 1341–1347.

Ritchey, M., Libby, L. A., & Ranganath, C. (2015). Cortico-hippocampal systems involved in memory and cognition: The PMAT framework. *Progress in Brain Research*, *219*, 45–64.

Sander, C. Y., Hooker, J. M., Catana, C., Normandin, M. D., Alpert, N. M., Knudsen, G. M., Vanduffel, W., Rosen, B. R., & Mandeville, J. B. (2013). Neurovascular coupling to D2/D3 dopamine receptor occupancy using simultaneous PET/functional MRI. *Proceedings of the National Academy of Sciences of the United States of America*, *110*(27), 11169–11174.

Schaefer, A., Kong, R., Gordon, E. M., Laumann, T. O., Zuo, X. N., Holmes, A. J., Eickhoff, S. B., & Yeo, B. T. T. (2018). Local-global parcellation of the human cerebral cortex from intrinsic functional connectivity MRI. *Cerebral Cortex*, *28*(9), 3095–3114.

Scheef, L., Spottke, A., Daerr, M., Joe, A., Striepens, N., Kolsch, H., Popp, J., Daamen, M., Gorris, D., Heneka, M. T., Boecker, H., Biersack, H. J., Maier, W., Schild, H. H., Wagner, M., & Jessen, F. (2012). Glucose metabolism, gray matter structure, and memory decline in subjective memory impairment. *Neurology*, *79*(13), 1332–1339.

Shulman, R. G., Hyder, F., & Rothman, D. L. (2001). Lactate efflux and the neuroenergetic basis of brain function. *NMR in Biomedicine*, *14*(7–8), 389–396.

van den Heuvel, M. P., de Lange, S. C., Zalesky, A., Seguin, C., Yeo, B. T. T., & Schmidt, R. (2017). Proportional thresholding in resting-state fMRI functional connectivity networks and consequences

for patient-control connectome studies: Issues and recommendations. *NeuroImage*, *152*, 437–449.

Viviano, R. P., Hayes, J. M., Pruitt, P. J., Fernandez, Z. J., van Rooden, S., van der Grond, J., Rombouts, S., & Damoiseaux, J. S. (2019). Aberrant memory system connectivity and working memory performance in subjective cognitive decline. *NeuroImage*, *185*, 556–564.

Wang, M., Jiang, J., Yan, Z., Alberts, I., Ge, J., Zhang, H., Zuo, C., Yu, J., Rominger, A., Shi, K., & I. Alzheimer's Disease Neuroimaging. (2020). Individual brain metabolic connectome indicator based on Kullback-Leibler divergence similarity estimation predicts progression from mild cognitive impairment to Alzheimer's dementia. *European Journal of Nuclear Medicine and Molecular Imaging*, *47*(12), 2753–2764.

Wang, X., Huang, W., Su, L., Xing, Y., Jessen, F., Sun, Y., Shu, N., & Han, Y. (2020). Neuroimaging advances regarding subjective cognitive decline in preclinical Alzheimer's disease. *Molecular Neurodegeneration*, *15*(1), 55.

Yu, M., Sporns, O., & Saykin, A. J. (2021). The human connectome in Alzheimer disease—relationship to biomarkers and genetics. *Nature Reviews. Neurology*, *17*(9), 545–563.

Zhao, Q., Sang, X., Metmer, H., Swati, Z., Lu, J., & I. Alzheimer's Disease NeuroImaging. (2019). Functional segregation of executive control network and frontoparietal network in Alzheimer's disease. *Cortex*, *120*, 36–48.

SUPPORTING INFORMATION

Additional supporting information can be found online in the Supporting Information section at the end of this article.

How to cite this article: Wang, L., Xu, H., Wang, M., Brendel, M., Rominger, A., Shi, K., Han, Y., & Jiang, J. (2023). A metabolism-functional connectome sparse coupling method to reveal imaging markers for Alzheimer's disease based on simultaneous PET/MRI scans. *Human Brain Mapping*, *44*(17), 6020–6030. https://doi.org/10.1002/hbm.26493